Gazi University Journal of Science
GU J Sci
26(2):279-302 (2013)

Comparison of Liquefaction Susceptibility Maps of Saruhanlı Town (Turkey) Based on Various Liquefaction Indices

Mehmet ORHAN[1], Nihat Sinan IŞIK[1], Mustafa ÖZER[1♠], Ali ATEŞ[2]

[1]*Gazi Unv., Faculty of Technology, Civil Engineering Department, 06500 Beşevler Ankara TURKEY.*

[2]*Düzce Unv., Faculty of Technology, Civil Engineering Department, 81620 Konuralp Düzce TURKEY.*

Received: 04.06.2013 Revised: 12.04.2013 Accepted:25.04.2013

ABSTRACT

In this study, liquefaction susceptibility maps of the Saruhanlı district of Manisa (Turkey) were prepared based on different methods for the evaluation of liquefaction potential and various liquefaction indices. Three main fault zones are present near the study area, namely Bergama, Buyuk Menderes, and Gediz Graben. The Gediz Graben controls the seismicity of the area. The total length of this fault zone is about 150 km, and it is about 33 km from the study site. By considering historical earthquakes within the Gediz Graben and its length, a design earthquake with a moment magnitude of 7.1 was selected for the study site. A peak ground acceleration of 0.28g was calculated for the study site using attenuation relationships developed for Turkey. In order to analyze liquefaction susceptibility of the Saruhanlı region, results from a total of 28 cone penetration tests (CPT) were evaluated. Four different CPT-based methods were used for the calculation of factor of safety against liquefaction. These factors of safety were used to define the liquefaction indices. Three different liquefaction indices were used to develop the liquefaction susceptibility maps of the area. Hence, a total of twelve liquefaction susceptibility maps were prepared to evaluate liquefaction potential of the area. In additon,

♠Corresponding author, e-mail:ozerm@gazi.edu.tr

liquefaction susceptibility maps were prepared using varying depths of the ground water table to determine the effect of seasonal ground water level changes on the liquefaction severity. Besides, liquefaction-induced ground settlement maps were also prepared for the study site.

Key words: Liquefaction, liquefaction susceptibility maps, liquefaction index, CPT, Saruhanlı.

1. INTRODUCTION

Turkey is one of the most seismically active countries in the world. Earthquakes in Turkey are generally associated with several active fault systems, namely the North Anatolian Fault Zone (NAFZ), East Anatolian Fault Zone (EAFZ) and the West Anatolian Fault System (WAFS) (Fig. 1). These fault systems have produced many devastating earthquakes. Most recent devastating earthquakes on this fault zone are the Düzce earthquake (M_s = 7.5) on November 12, 1999; the Kocaeli-Gölcük earthquake (M_s = 7.8) on August 17, 1999; the Ceyhan-Adana earthquake (M_s = 6.2) on June 27, 1998; the Dinar earthquake (M_s = 6.1) on November 1, 1995; and the Erzincan earthquake (M_s = 6.8) on March 13, 1992 [1]. These earthquakes severely damaged or destroyed many buildings and lifelines and caused many deaths. Liquefaction and associated ground failures were widely observed during these earthquakes.

While liquefaction phenomenon have occurred in many earthquakes in Turkey, liquefaction gained importance among the geotechnical community after the 1992 Erzincan earthquake, and especially after the 1999 Adapazari (Turkey) earthquake, in which soil liquefaction was widely observed. During the site selection and planning stages for settlement areas and engineering structures, the evaluation of the liquefaction potential of a liquefaction-prone area is one of the important tasks in geotechnical earthquake engineering. In this respect, preparation of liquefaction susceptibility maps is an important stage of the site selection and planning stages.

Two main tasks should be fulfilled to prepare liquefaction susceptibility map of an area. The first task is to calculate the factors of safety against liquefaction using a proper liquefaction evaluation method, and the second task is to calculate liquefaction index based on a suitable method using the factors of safety against liquefaction. There are many methods based on in-situ tests to calculate factors of safety against liquefaction and three methods to calculate liquefaction severity index.

In this study, liquefaction susceptibility maps of the Saruhanlı district of Manisa (Turkey) were prepared based on different liquefaction evaluation methods and various liquefaction indices. Four popular methods were used to calculate the factor of safety against liquefaction, and three methods were used for the determination of liquefaction severity index. Hence, a total of twelve liquefaction susceptibility maps were prepared to evaluate liquefaction potential of the area. Besides, liquefaction susceptibility maps that reflect the effect of fluctuations of the ground water table (GWT) due to seasonal changes on the liquefaction potential were constructed using varying depths of the GWT. In addition, liquefaction-induced ground settlement maps were also prepared for the study site. These maps may assist structural and geotechnical engineers to identify areas where liquefaction potential is likely when designing new buildings and retrofitting existing structures.

2. DESCRIPTION OF THE STUDY SITE

2.1. Geography and Urbanization

Saruhanlı is a town in the city of Manisa that is about 19 km northeast of the city center and situated in the Aegean Region of Turkey (Fig. 1). Saruhanlı is located within the Gediz Valley, which consists mainly of alluvial deposits of the Gediz River and is bounded by normal faults. The topography is almost flat, and the elevation is about 40 meters. The current population of Saruhanlı is about 64134 and is increasing. This increase has revealed the necessity of a new settlement area. In order to meet the demand, extending the existing settlement area has been proposed by the government of the city. The site evaluated in this study includes an existing settlement area as well as a proposed settlement area (Fig. 2). The area of the existing settlement site and the study site including the existing settlement area are about 3 and 12 km^2, respectively.

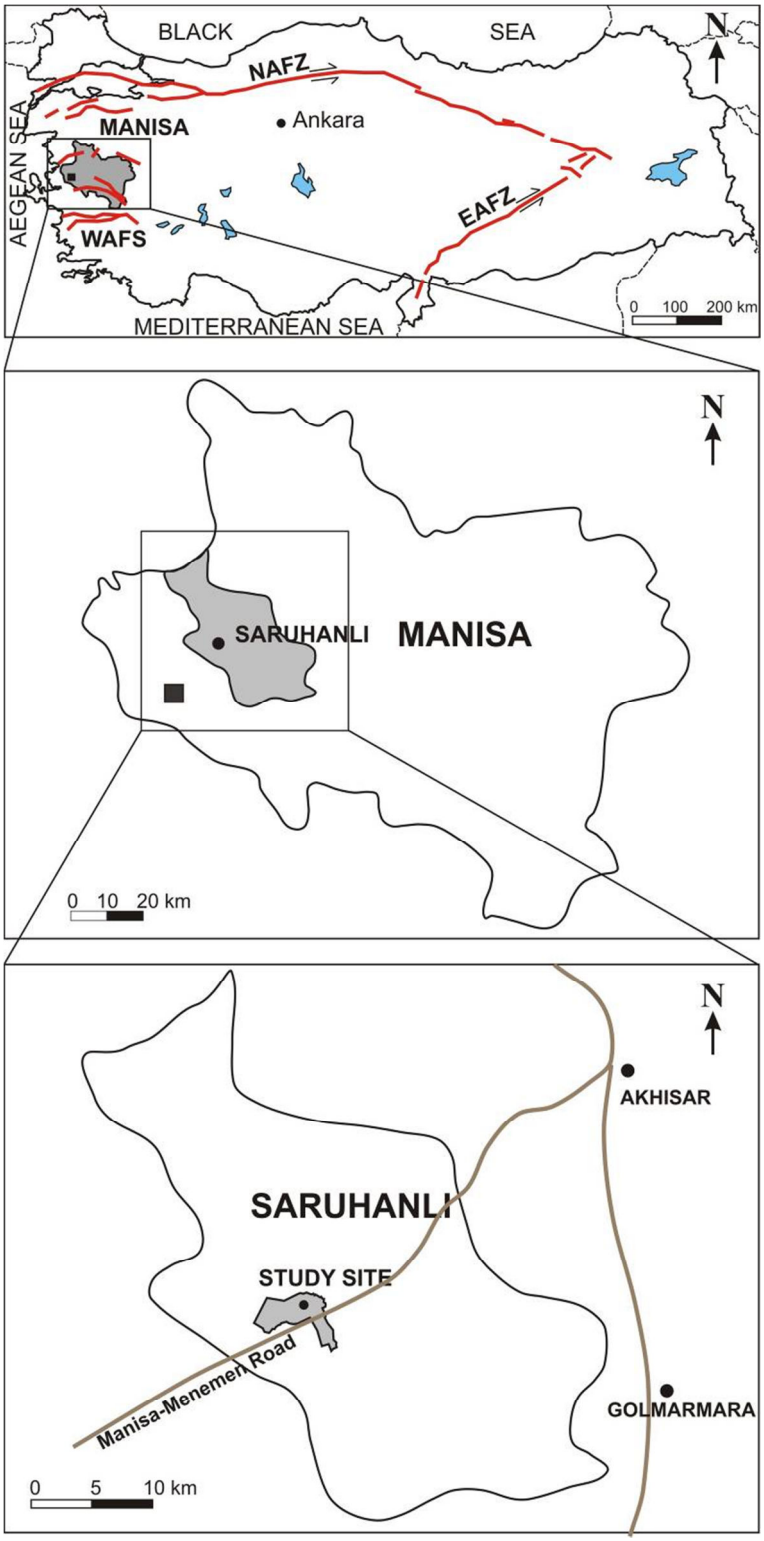

Figure 1. Location maps of the study site in the Saruhanlı-Manisa area of Turkey (NAFZ: North Anatolian Fault Zone, EAFZ: East Anatolian Fault Zone, WAFZ: West Anatolian Fault System).

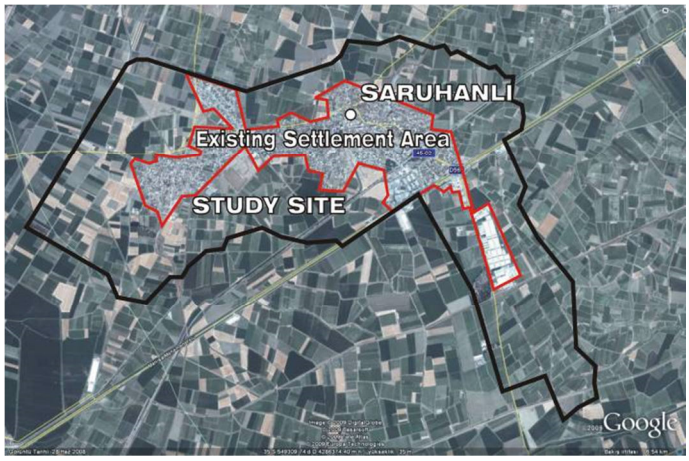

Figure 2. A view of satellite image of the study site and the existing settlement area.

2.2. Geological Setting of the Study Area

The Gediz graben is the most prominent and the best developed graben basin in western Turkey [2]. The rock units exposed in the vicinity of the Gediz graben can be classified into two groups; the basement and the overlying cover units (Figure 3). The metamorphic rocks belonging to the Menderes Massif constitute the pre-Neogene basement and are exposed extensively over the horst blocks that rise to an elevation of approximately 2000 m [2]. The graben-fill rest structurally over the metamorphic rocks of the Menderes Massif along a low-angle normal fault (Gediz detachment); a metamorphic core complex composed of deep metamorphic rocks and associated granites [3]. The fill of the Gediz graben comprises Miocene to recent continental clastics of mainly lacustrine, alluvial and fluvial origin [3].

Pliocene-aged detritical conglomerates, sandstones, siltstones, claystones and Quaternary alluvial deposits are exposed within Saruhanlı and the vicinity (Figure 4).

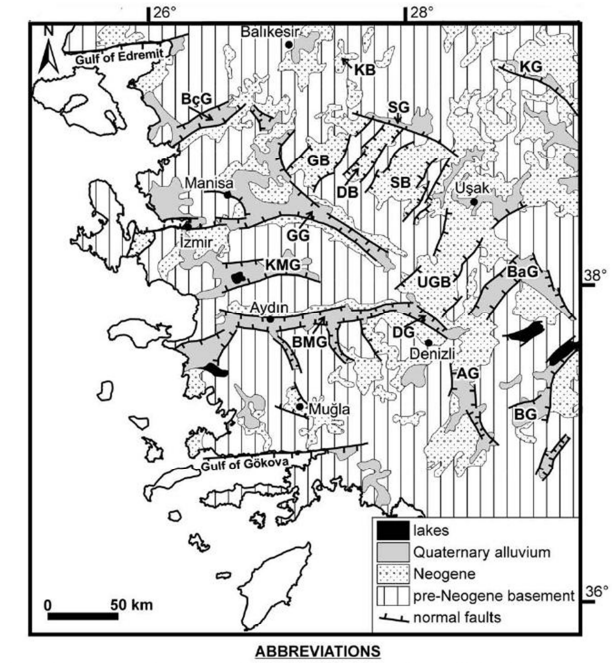

ABBREVIATIONS

AG : Acıpayam Graben	DB : Demirci Basin	KG :Kütahya Graben
BçG : Bakırçay Graben	DG : Denizli Graben	KMG: Küçük Menderes Graben
BaG : Baklan Graben	GB : Gördes Basin	SB : Selendi Basin
BG : Burdur Graben	GG : Gediz Graben	SG : Simav Graben
BMG: Büyük Menderes Graben	KB : Kavacık Basin	UGB: Uşak-Güre Basin
NAFS: North Anatolian Fault System		EAFS: East Anatolian Fault System

Figure 3. Tectonic setting and simplified geological map of SW Turkey [2].

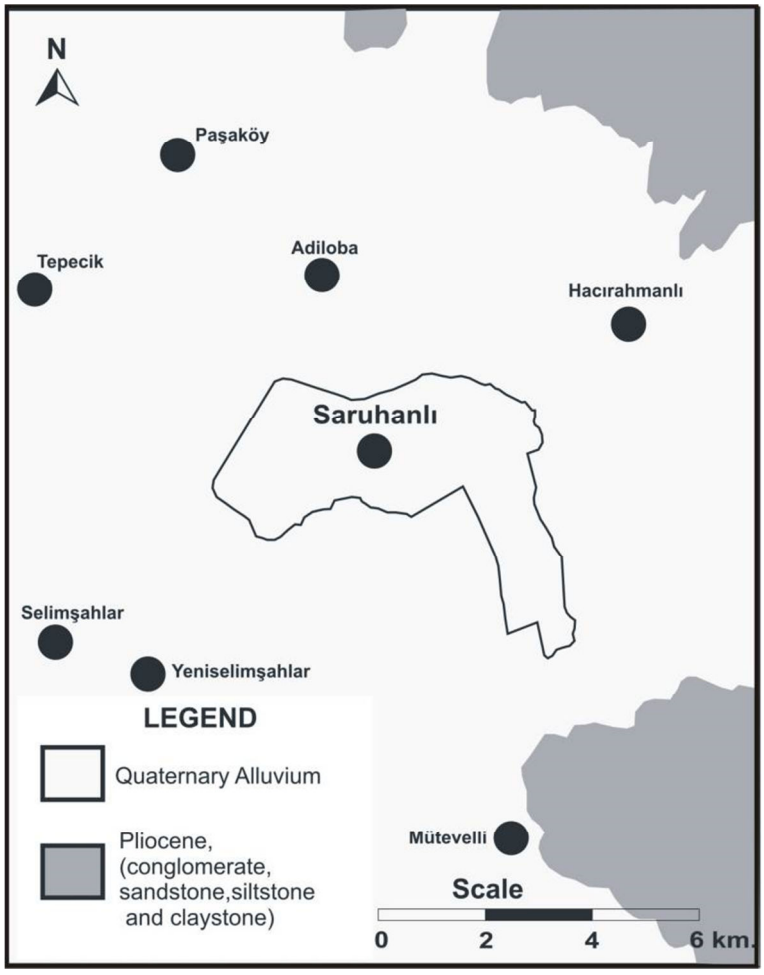

Figure 4. Geological map of Saruhanlı and its vicinity (arranged from Metli et al., 2001 [4]).

Based on seismic refraction studies performed and boreholes drilled 85 km southeast of Saruhanlı, the depth of the metamorphic basement rocks is about 1750 m [5], but it becomes significantly shallower towards the boundary of the normal faults of the Gediz graben [5]. The thickness of the sedimentary fill at the north side of the Gediz graben is less than that at the south side [5].

2.3. Seismotectonics and Seismicity

West Anatolia is one of the most active extensional regimes of the world. This region developed under a compression then tensional Cenozoic tectonic regime. The tensional regime, which has been achieve since the Upper Miocene, resulted in the formation of large grabens, namely the Buyuk Menderes, Kucuk Menderes and Gediz [6]. These normal faults also control the geomorphology of the Aegean region.

The Gediz graben lies between the towns of Alasehir and Salihli, Manisa in the NE–SW direction. It is an arc shaped structure about 150 km in length and 3 to 30 km wide. The most seismically active and largest faults of the Gediz graben are located along its southern margin [2]. The normal faults of the Gediz graben control the seismicity of Saruhanlı and its vicinity. Figure 5 shows the active faults and epicenters in the study area.

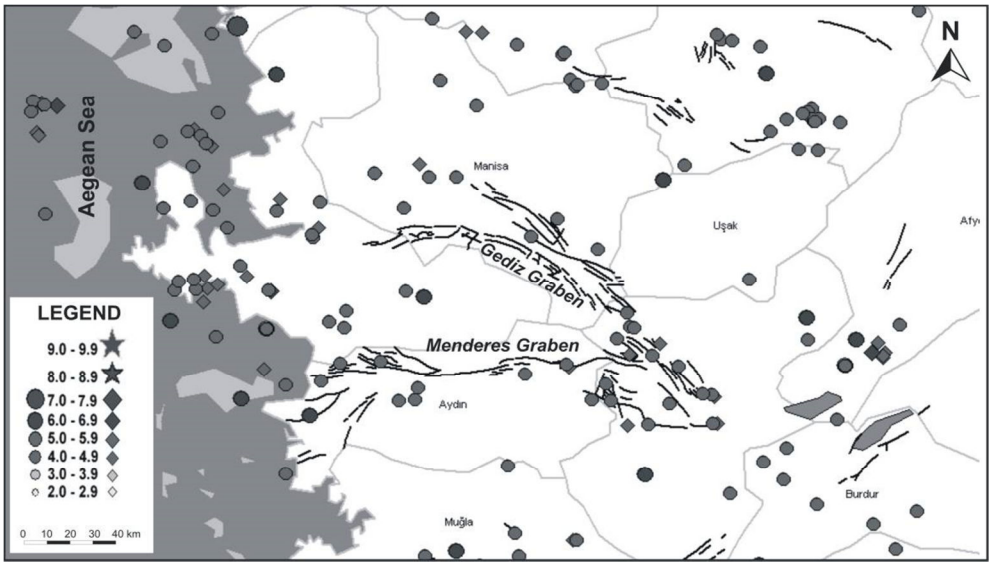

Figure 5. Distributions of the epicenters and active faults in the study area [7].

Because of the neotectonics of Western Anatolia, the majority of the earthquakes in this region are associated with normal faulting. Within the Aegean Extensional Province, 33 damaging earthquakes have occurred along normal faults. Among these; the Burdur (1914) and Gediz (1970) earthquakes had magnitudes greater than 7 on the Richter scale. Figure 5 presents the distribution of the earthquake epicenters in the region of the study site.

In order to assess the liquefaction potential of the study site and prepare liquefaction susceptibility maps, moment magnitude (M_w) and peak-horizontal ground acceleration (PGA) should be estimated.

As stated previously, there are three major fault systems around the study site; these are the Buyuk Menderes, Bergama and Gediz Grabens, with lengths of 200, 60, and 150 km, respectively. The closest distances of these fault systems to the Saruhanlı region are about 100, 37, and 33 km, respectively (Fig. 6). The Gediz Graben is the closest and longest of the fault systems. For this reason, it can be argued that the Gediz Graben controls the seismicity of the region.

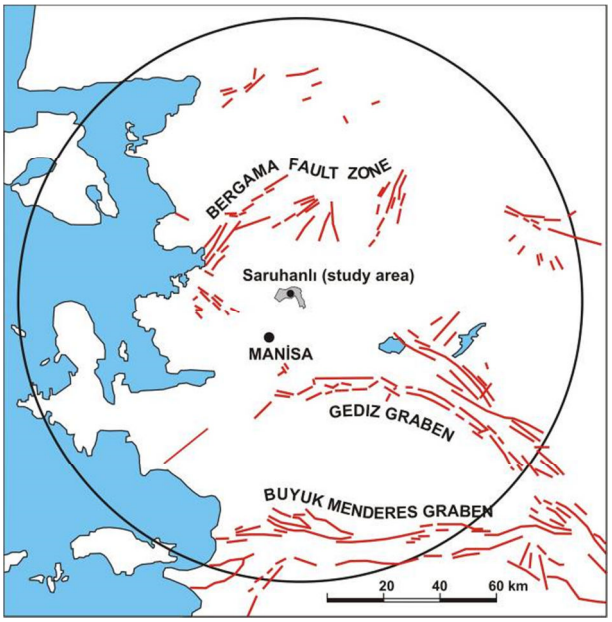

Figure 6. Main fault zones that affect the study area (radius of circle is 100 km).

The moment magnitude of the design earthquake was estimated by using the empirical equation (Eq. 1) proposed by Wells and Coppersmith (1994) [8].

$$M_w = 4.86+1.32\ \mathrm{Log}L \quad (1)$$

where M_w is the moment magnitude of the design earthquake and L is the fault length that is considered to rupture during the earthquake. The moment magnitude of the design earthquake is calculated as 7.1 by assuming 50 km length of the Gediz Graben will rupture. Actually the length of individual segments of Gediz Graben should be used for the estimation of the moment magnitude. However since the segments are not clearly investigated, it was assumed that 1/3 of the Gediz Graben may rupture.

For the determination of the PGA at the study site, the empirical attenuation relationship (Eq. 2) proposed by Ulusay et al. (2004) [9] was employed. This relationship was developed using the ground motions recorded in Turkey between the years 1976 and 2003; therefore, this regional attenuation relation was preferred.

$$a_{max} = 2.18e^{0.0218(33.3M_w - R_e + 7.8427S_A + 18.9282S_B)} \quad (2)$$

where a_{max} is the peak-horizontal ground acceleration (gal), M_w is the moment magnitude of the earthquake (dimensionless), R_e is the distance to the epicenter (km), and S_A and S_B are the site condition constants (S_A=0 and S_B = 0 for rock site, S_A=1, S_B = 0 for soil site, S_A=0, S_B = 1 for soft soil site). The CPT results indicated that the layers forming the soil profile could be described as "soft soil". Therefore, for the values of M_w = 7.1, R_e = 33 km, and S_A=0 and S_B = 1, a_{max} of 278 gal (0.28g) was estimated for the study site.

3. GEOTECHNICAL INVESTIGATIONS

In order to evaluate the liquefaction potential of soils, simplified methods using in-situ tests, originated by Seed and Idriss (1971) [10], are widely used. The in-situ tests commonly employed for liquefaction evaluation are the standard penetration test (SPT), cone penetration test (CPT) and shear wave velocity test (V_s). Compared with the other two tests, CPT has the advantages of greater accuracy and repeatability. In addition, continuous profiles of soil parameters can be obtained with CPT, and thus it is more suitable for studying soil characteristics and liquefaction potential [11]. For this reasons, CPT measurements were used to evaluate the liquefaction potential of soils within the study site.

3.1. Field Investigations

CPT soundings were carried out by İller Bankası [12] during the geological-geotechnical investigation of the study site. In this context, 28 CPT soundings were evenly distributed throughout the study site. In addition, four soil exploration trenches having approximately 4.5 meters depth were excavated. The locations of the CPTs and trenches are depicted in Fig. 7.

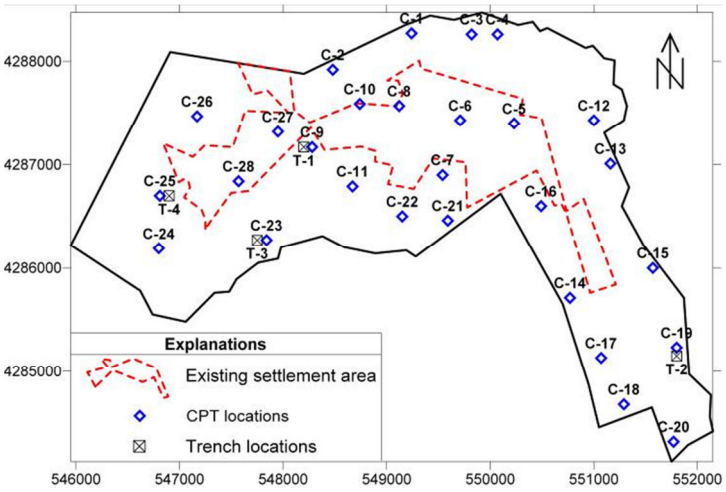

Figure 7. Location map of the CPT soundings and soil investigation trenches.

Depending on the depth of very dense-coarse grained strata, the CPT soundings were carried out to depths varying between 6.50 and 12.50 m. During the CPT soundings, tip resistance, friction resistance and pore water pressure were measured at 25 mm intervals. A selected CPT sounding log illustrating the CPT tip and friction resistance with depth and the position of the groundwater table are given in Fig. 8. According to the

excess pore water pressures measured during the CPT soundings, as well as borehole measurements and observations in the soil exploration trenches the depth of the groundwater table varies between 0 and 4.5 meters with an average value of 3 meters. Fig. 9 shows a sample photograph of a selected trench. Since the study area is almost flat, the difference between the measured depths of the water table is exhibited small local variations.

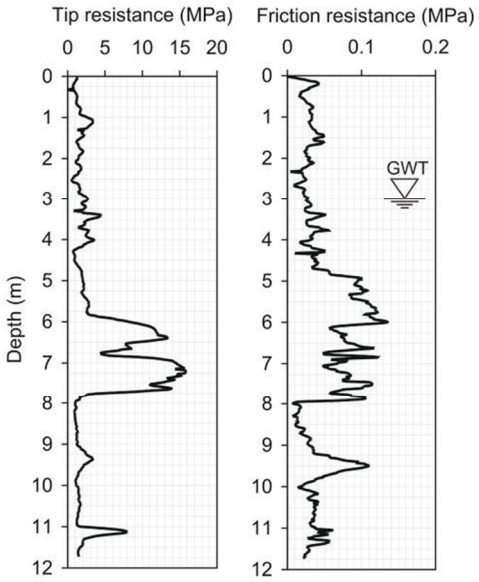

Figure 8. Example CPT sounding log illustrating the subsurface conditions at the study site.

Figure 9. A view of a selected soil investigation trench showing running sands due to water flow.

3.2. Laboratory Investigations

Disturbed samples were recovered from the trenches and were tested by the authors to determine particle size distribution, Atterberg limits and other index properties. All laboratory tests were performed in the soil mechanics laboratory of the Gazi University Faculty of Technology according to relevant ASTM standards. Results obtained from these samples indicated that the soils are mainly SM – SC types according to Unified Soil Classification System (USCS) and are all non-plastic. Clay contents (particle diameter ≤ 5 μm) range between 2 % and 12 %. Figure 10 shows particle size distribution curves of samples recovered from trenches and well-established boundaries for liquefiable soils suggested by Tsuchida (1970) [13]. As is clear from Figure 10, the particle size distributions of soils recovered from the trenches mainly fall between the liquefiable boundaries.

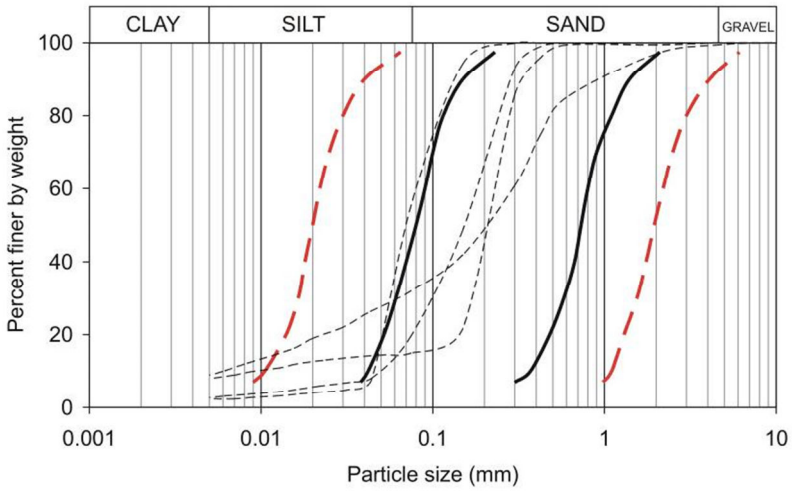

Figure 10. Particle size distributions of the tested soils with the boundaries of liquefiable soils suggested by Tsuchida (1970) [13] (Dashed-thick lines indicate the boundaries of potentially liquefiable soils, while solid-thick lines indicate the boundaries of the most liquefiable soils and the other lines, "dashed-thin ones" indicate the tested soils).

4. CALCULATION OF LIQUEFACTION POTENTIAL OF SOILS

Calculation or estimation of two quantities is required for the evaluation of liquefaction potential of soils. These quantities are the seismic demand placed on a soil layer by a given earthquake, expressed in terms of the cyclic stress ratio (CSR), and the capacity of the soil to resist liquefaction, expressed in terms of the cyclic resistance ratio (CRR) [14]. The CRR reflects the resistance of the soil, whereas the CSR characterizes the power of the earthquake. The term CRR may be considered as the maximum CSR that a soil can resist before liquefying. Hence, the ratio of the CRR to the CSR gives the factor of safety (F_s) of the soil against liquefaction (Eq. 3). The higher the F_s, the more resistant the soil is against liquefaction.

$$F_S = \frac{\mathrm{CRR}}{\mathrm{CSR}} \tag{3}$$

In order to estimate the CSR caused by a given earthquake, a basic simplified equation was developed by Seed and Idriss (1971) [10]. The equation is widely used worldwide with some adjustments. The simplified method for the calculation of CRR was also first developed by Seed and Idriss (1971) [10] based on the standard penetration test (SPT). Thereafter, many simplified methods were developed based on different in-situ tests (e.g., CPT, BPT and shear wave velocity). In this study, four widely-used CPT-based methods were employed to calculate the CRR; these are the Robertson and Wride (1998) [15], the Boulanger and Idriss (2004) [16], the Juang et al. (2006) [17], and the Moss et al. (2006) [18] methods. Calculation procedures for determining CSR and CRR that were employed in this study were briefly summarized in following sections.

4.1. Calculation of CSR

The simplified equation originated by Seed and Idriss (1971) [10] for calculating CSR is used currently with some refinements. The equation developed by Seed and Idriss (1971) [10] is mainly adjusted to the benchmark earthquake (M_w = 7.5). The final equation that was used in this study is as follows:

$$\mathrm{CSR}_{7.5} = \left[0.65 \left(\frac{a_{\max}}{g} \right) \left(\frac{\sigma_{\mathrm{vo}}}{\sigma'_{\mathrm{vo}}} \right) r_d \right] / \mathrm{MSF}/K_\sigma \tag{4}$$

where a_{max} is the peak-horizontal ground acceleration at the ground surface generated by the earthquake (m/s^2), g is the acceleration of gravity (9.81 m/s^2), σ_{vo} and σ'_{vo} are the total and effective vertical overburden stresses at the depth studied, respectively (kN/m^2), r_d is the shear stress reduction factor (dimensionless), MSF is the magnitude scaling factor (dimensionless), and K_σ is the overburden correction factor (dimensionless). Detailed information about the terms r_d, MSF, and K_σ can be obtained from Youd et al. (2001) [14].

4.2. Calculation of CRR

Robertson and Wride (1998) method

In the Robertson and Wride (1998) [15] method, CRR is calculated by the following equations;

$$\mathrm{CRR} = 0.833\left[\frac{(q_{c1N})_{cs}}{1000}\right] + 0.05 \text{ if } (q_{c1N})_{cs} < 50 \quad (5a)$$

$$\mathrm{CRR} = 93\left[\frac{(q_{c1N})_{cs}}{1000}\right]^3 + 0.08 \text{ if } 50 \le (q_{c1N})_{cs} < 160 \quad (5b)$$

where $(q_{c1N})_{cs}$ is the clean-sand cone penetration resistance normalized to a reference stress level of one atmosphere. The normalization process, which converts the measured cone tip resistance (q_c) to the normalized cone tip resistance (q_{c1N}), and the procedure to determine the clean-sand equivalence $(q_{c1N})_{cs}$ from q_{c1N}, are described in detail in [15]. An important parameter of the normalization process is the stress exponent n. Because a somewhat discontinuous variation of n was applied in Robertson and Wride (1998) [15], a new set of values of the stress exponent for normalizing cone penetration resistance was proposed by Robertson (1999) [19] to produce a smoother variation of n for soils from clean sands to clays. The new values of n for clean sands and clays are the same as those used in Robertson and Wride (1998) [15] and are only different for silty soils [20]. In this study, the new set of values of the stress exponent, n, proposed by Robertson (1999) [19] was used for normalizing cone penetration resistance and hence calculating the CRR.

In the Robertson and Wride (1998) [15] method, the terms r_d, MSF, and K_σ are calculated with the formulae recommended by the NCEER workshop [14]. Therefore, the formulae proposed by Liao and Whitman (1986) [21] for r_d, Seed and Idriss (1982) [22] for MSF (revised version of original formula), and Hynes and Olsen (1999) [23] for K_σ were utilized. These equations are as follows:

$$r_d = 1.0 - 0.00765z \text{ for } z \le 9.15 \text{ m} \quad (5c)$$

$$r_d = 1.174 - 0.0267z \text{ for } 9.15 \text{ m} < z \le 23 \text{ m} \quad (5d)$$

$$\mathrm{MSF} = 10^{2.24}/M_w^{2.56} \quad (5e)$$

$$K_\sigma = (\sigma'_{vo}/P_a)^{(f-1)} \quad (5f)$$

where z is the depth (in m), M_w is the moment magnitude (dimensionless), P_a is the atmospheric pressure (approximately 100 kPa), and f is an exponent that is a function of site conditions, including relative density, stress history, aging, and overconsolidation ratio. For relative densities between 40 and 60%, $f = 0.7 - 0.8$; for relative densities between 60 and 80%, $f = 0.6 - 0.7$.

Boulanger and Idriss (2004) method

In the Boulanger and Idriss (2004) method, CRR is calculated as follows:

$$\mathrm{CRR} = \exp\left\{\frac{q_{c1N}}{540} + \left(\frac{q_{c1N}}{67}\right)^2 - \left(\frac{q_{c1N}}{80}\right)^3 + \left(\frac{q_{c1N}}{114}\right)^4 - 3\right\} \quad (6)$$

where q_{c1N} is the CPT tip resistance corrected to an equivalent overburden stress of one atmosphere and then divided by atmospheric pressure to eliminate units (i.e., $q_{c1N} = q_{c1}/P_a$). The correction process of the CPT tip resistance is described in detail in Boulanger and Idriss (2004) and Idriss and Boulanger (2006).

In the Boulanger and Idriss (2004) [16] method, the terms r_d, MSF, and K_σ are calculated as follows [24]:

$$\ln(r_d) = \alpha + \beta M_w \quad (6a)$$

$$\alpha = -1.012 - 1.126 \sin(5.133 + z/11.73) \quad (6b)$$

$$\beta = 0.106 + 0.118 \sin(5.142 + z/11.28) \quad (6c)$$

$$\mathrm{MSF} = -0.058 + 6.9 \exp(-M_w/4) \le 1.8 \quad (6d)$$

$$K_\sigma = 1 - C_\sigma \ln(\sigma_v/P_a) \le 1.0 \quad (6e)$$

$$C_\sigma = 1/[37.3 - 8.27(q_{c1N})^{0.264}] \quad (6f)$$

where z is the depth (m), M_w is the moment magnitude (dimensionless) and P_a is the atmospheric pressure.

Juang et al. (2006) method

In the Juang et al. (2006) [17] method, CRR is calculated as:

$$\mathrm{CRR} = \exp\{-2.9439 + 0.000309 + (q_{c1N,m})^{1.8}\} \quad (7)$$

where $q_{c1N,m}$ is the stress-normalized cone tip resistance q_{c1N} adjusted for the effect of "fines" on liquefaction (thus, $q_{c1N,m}=Kq_{c1N}$). The stress-normalized cone tip resistance q_{c1N} used by Juang et al. (2006) [17] follows the definition by Boulanger and Idriss (2004) [16]. The definition of the adjustment factor K and other calculation details are available in Juang et al. (2006) [17].

In the Juang et al. (2006) [17] method, the terms r_d, MSF, and K_σ are calculated with the equations recommended by Boulanger and Idriss (2004) [16].

Moss et al. (2006) method

In the Moss et al. (2006) [18] method, the CRR for a given probability of liquefaction can be calculated from Eq. 8.

$$\mathrm{CRR} = \exp\left\{\frac{(q_{c1})^{1.045} + q_{c1}(0.110R_f) + (0.001R_f) + c(1+0.850R_f) - (0.848\ln M_w) - (0.002\ln\sigma'_v) - 20.923 + 1.632\Phi^{-1}(P_L)}{7.177}\right\} \quad (8)$$

In Eq.8; q_{c1} is the normalized tip resistance (MPa); R_f is the friction ratio (percent); c is the normalization exponent; σ'_v is the effective overburden stress (kPa); and $\Phi^{-1}(P_L)$ is the inverse cumulative normal distribution function. A brief discussion of CPT normalization for effective overburden stress can be found in Moss et al. (2006) [18].

Moss et al. (2006) [18] used the Çetin et al. (2004) [25] formulae for r_d and MSF (these terms was called the nonlinear shear mass participation factor and the magnitude-correlated duration weighting factor, respectively, in Çetin et al. (2004) [25] study; however, for convenience, this factors is called the magnitude scaling factor "MSF" and the shear stress reduction factor "r_d", respectively, in this study). The K_σ correction was not applied by the Moss et al. (2006) [18]. The terms r_d and MSF are calculated by the following equations:

$$r_d = \left[\frac{\left(1+\frac{-9.147-4.173\cdot a_{max}+0.652\cdot M_w}{10.567+0.089\cdot e^{0.089\cdot(-d\cdot 3.28-7.760\cdot a_{max}+78.576)}}\right)}{\left(1+\frac{-9.147-4.173\cdot a_{max}+0.652\cdot M_w}{10.567+0.089\cdot e^{0.089\cdot(-7.760\cdot a_{max}+78.576)}}\right)}\right] \quad (8a)$$

$$\mathrm{MSF} = 17.84\cdot(M_w)^{-1.43} \quad (8b)$$

where d is the depth at the midpoint of the critical layer (m); M_w is the moment magnitude (dimensionless); and a_{max} is the peak-horizontal ground acceleration at the ground surface (in units of gravity). Eq. 8b is valid for only M_w = 5.5–8.5.

5. CALCULATION OF LIQUEFACTION INDEX

As previously mentioned, various methods based on different in situ tests have been proposed by many researchers to evaluate the liquefaction potential of soils. The factor of safety (F_s) against liquefaction of a soil layer at a particular depth can be obtained from these methods. However, when considering the liquefaction potential of a site, F_s is not adequate alone for the evaluation of liquefaction potential and ground failure risk. In order to overcome this limitation, the liquefaction potential index I_L, which takes into account the thickness, depth and F_s value of the liquefiable soil layers, was first proposed by Iwasaki et al. (1982). The overall liquefaction potential of all the soil layers at a profile can be evaluated with this index. Due to its ease of use, I_L is widely used for the evaluation of the ground failure risk and particularly for mapping the liquefaction susceptibility of an area. Similar indices under different names were later suggested by different investigators. These indices that are used in this study were briefly summarized below.

5.1. Liquefaction Potential Index I_L Proposed by Iwasaki et al (1982)

The liquefaction potential index I_L, proposed by Iwasaki et al. (1982) [26], is defined as follows:

$$I_L = \sum_0^{20} F_1 W(z)\mathrm{dz} \quad (9)$$

where F_1 is an index defined as given in Eqs. 9a and 9b; and W(z) is a weight function of the depth defined as given in Eqs. 9c and 9d.

$F_1 = 1 - F_s$ if $F_s < 1$ (9a)

$F_1 = 0$ if $F_s \geq 1$ (9b)

$W(z) = 10 - 0.5z$ if $z < 20$ (9c)

$W(z) = 0$ if $z > 20$ (9d)

where z is the depth of the mid-point of the soil layer in meters, and F_s is the factor of safety against liquefaction. The F_s used by Iwasaki et al. (1982) [26] for developing the liquefaction potential index was obtained from a SPT-based simplified method that is specified in the Japanese Highway Bridge Design Code [27]. Iwasaki et al. (1982) [26] provided a liquefaction risk criteria based on a database of 64 liquefied sites and 23 non-liquefied sites from six earthquakes [11]. These criteria are given in Table 1.

Table 1. Iwasaki criteria for the evaluation of liquefaction failure potential of soils [26].

Liquefaction potential index (I_L)	Liquefaction failure potential
$I_L = 0$	Extremely low
$0 < I_L < 5$	Low
$5 < I_L < 15$	High
$15 > I_L$	Extremely high

5.2. Liquefaction Risk Index I_R Proposed by Lee et al. (2003)

Lee et al. (2003) [11] analyzed data from 72 CPT soundings and field observations obtained from the Yuanlin area, where extensive soil liquefaction was observed after the 1999 Chi-Chi earthquake, and proposed a new liquefaction index; they called this index the liquefaction risk index (I_R). Lee et al. (2003) [11] used the same equation suggested by Iwasaki et al. (1982) [26] except but replaced the F_1 term with the P_L term, which is a probability function suggested by Juang et al. (2003) [28]. The index I_R proposed by Lee et al. (2003) [11] is defined as follows:

$$I_R = \sum_{0}^{20} P_L \, W(z)\mathrm{dz} \tag{10}$$

where P_L is the probability of liquefaction suggested by Juang et al. (2003) [28] and can be obtained from Eq. 10a; W(z) is a weight function of the depth as previously defined in equations 9c and 9d.

$$P_L = \frac{1}{1+(F_s/0.96)^{4.5}} \tag{10a}$$

Lee et al. (2003) [11] used the Juang et al. (2003) [28] method to analyze the CPT data during development of the I_R. Hence, they used the value of 2.38 for the upper bound of the soil classification index I_c for liquefiable soils in the calculation of F_s values. Therefore, in this study, the value of 2.38 for I_c was used for the calculation of F_s values in conjunction with the Juang et al. (2006) [28] method.

Lee et al. (2003) [11] proposed three categories for I_R using the liquefaction map of the Yuanlin area. These categories are given in Table 2.

Table 2. The criteria proposed by Lee et al. (2003) for the evaluation of liquefaction failure potential of soils [11].

Liquefaction risk index (I_R)	Liquefaction failure potential
$I_R < 20$	Low
$20 < I_R \leq 30$	High
$30 > I_R$	Extremely high

5.3. Liquefaction Severity Index I_S Proposed by Sönmez and Gökceoğlu (2005)

Sönmez and Gökceoğlu (2005) [29] modified the categories suggested by Iwasaki et al. (1982) [26] and Lee et al. (2003) [11], respectively. Sönmez and Gökceoğlu (2005) [29] argued that non-liquefiable areas could not be distinguished due to the limited number of categories proposed by Lee et al. (2003) [11] and the category of ‘‘moderate’’ also lacks. Therefore, they modified the categories proposed by Lee et al. (2003) [11] by keeping the equations suggested by Lee et al. (2003) [11] the same. During modification of the categories, Sönmez and Gökceoğlu (2005) [29] accepted F_s = 1.411 for upper boundary of the liquefaction. After these modifications, Sönmez and Gökceoğlu (2005) [29] re-named the liquefaction risk index I_R as liquefaction severity index I_S. The new index I_S is calculated as follows:

$$I_S = \sum_{0}^{20} P_L \, W(z)\mathrm{dz} \tag{11}$$

$$P_L = \frac{1}{1+(F_s/0.96)^{4.5}} \quad \text{for } F_s \leq 1.411 \tag{11a}$$

$$P_L = 0 \quad \text{for} \quad F_s > 1.411 \tag{11b}$$

where P_L is the probability of liquefaction suggested by Juang et al. (2003) [28]; W(z) is a weight function of the depth, which can be obtained from equations 9c and 9d; and F_s is the factor of safety against liquefaction. The new categories suggested by Sönmez and Gökceoğlu (2005) [29] are given in Table 3.

Table 3. Liquefaction severity classification suggested by Sönmez and Gökceoğlu (2005) [29].

Liquefaction severity index (I_S)	Liquefaction failure potential
$I_S = 0$	Non-liquefied
$0 < I_S < 15$	Very low
$15 \leq I_S < 35$	Low
$35 \leq I_S < 65$	Moderate
$65 \leq I_S < 85$	High
$85 \leq I_S < 100$	Very high

6. CONSTRUCTION OF LIQUEFACTION SUSCEPTIBILITY MAPS

Liquefaction susceptibility maps of the study area (Saruhanlı, Turkey) were prepared based on both three indices (I_L, I_R, and I_S) in conjunction with four different CPT-based methods mentioned previously. During the liquefaction potential calculation (i.e. F_s values against liquefaction), the depth of the groundwater table was taken as 3 meters as explained previously.

6.1. Liquefaction Susceptibility Maps Based on Iwasaki et al. (1982) Method

The liquefaction potential indices (I_L) calculated with the Equation (Eq. 9) for all 28 CPT profiles in conjunction with four different CPT-based methods are listed in Table 4. The liquefaction susceptibility maps prepared based on data listed in Table 4 are presented in Fig. 11. The range of liquefaction index in Fig.11 was selected according to the boundary values of Iwasaki’s criteria (Table 1).

Table 4. Liquefaction potential indices (I_L) calculated using four different CPT based methods.

CPT No	CPT coordinates		Liquefaction potential index, I_L			
	X	Y	Robertson & Wride (1998)	Boulanger & Idriss (2004)	Juang et al. (2006)	Moss et al. (2006)
1	549240	4288270	2.37	4.04	2.88	3.94
2	548480	4287920	0.46	1.01	0.71	1.14
3	549820	4288260	2.75	4.05	2.82	4.43
4	550070	4288260	3.74	5.72	3.87	7.31
5	550230	4287400	4.45	5.97	4.29	4.08
6	549710	4287430	1.44	3.42	2.70	3.97
7	549540	4286900	3.01	4.16	2.53	3.70
8	549120	4287570	3.47	5.31	4.16	6.48
9	548280	4287170	2.27	3.53	2.91	4.47
10	548740	4287590	2.34	3.51	2.53	4.34
11	548670	4286790	0.74	2.00	1.15	1.63
12	551000	4287430	4.13	4.87	2.94	4.84
13	551160	4287010	0.53	1.35	0.41	1.14
14	550770	4285710	3.76	5.23	4.05	5.21
15	551570	4286000	1.16	1.84	1.06	1.20
16	550490	4286600	0.11	0.50	0.11	0.60
17	551070	4285130	0.83	2.06	1.15	2.66
18	551290	4284680	0.99	2.20	1.52	2.17
19	551800	4285230	0.18	1.36	0.00	1.87
20	551770	4284320	0.35	0.77	0.10	0.70
21	549590	4286460	0.83	1.73	1.05	1.88
22	549150	4286500	0.65	1.64	1.14	1.39
23	547840	4286270	0.97	2.46	0.68	1.79
24	546800	4286190	1.21	1.79	1.54	2.18
25	546810	4286700	2.45	4.11	2.36	4.80
26	547170	4287470	0.48	1.70	0.45	2.21
27	547950	4287320	3.08	4.52	2.47	5.04
28	547570	4286840	0.87	1.01	1.31	2.35

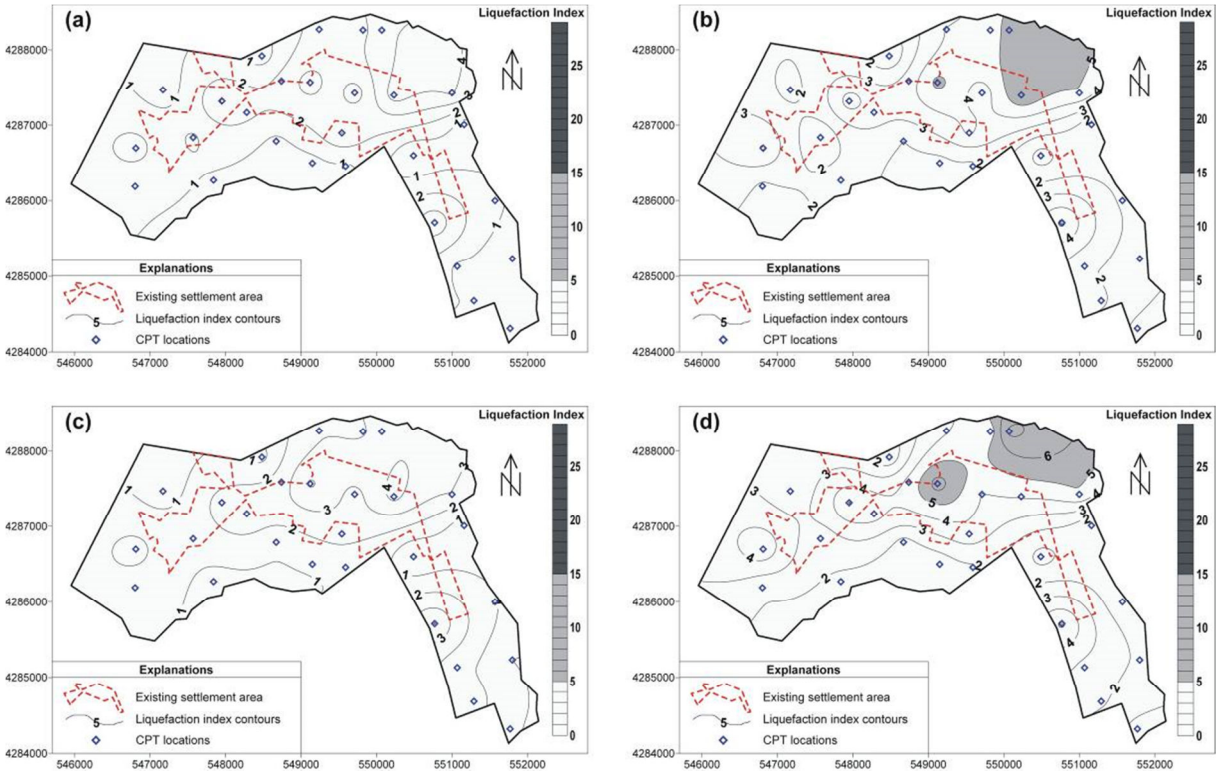

Figure 11. Liquefaction susceptibility maps based on Iwasaki's liquefaction potential index in conjunction with the (a) Robertson and Wride (1998) [15]; (b) Boulanger and Idriss (2004) [16]; (c) Juang et al. (2006) [17]; and (d) Moss et al. (2006) [18] methods.

As shown in Figs. 11(a) and 11(c), which were prepared using the F_s obtained by the Robertson and Wride (1998) [15] and Juang et al. (2006) [17] methods, respectively, the entire study area is classified as "low" according to liquefaction failure potential category suggested by Iwasaki et al. (1982) [26]. However, in the map constructed using the F_s obtained by Boulanger and Idriss (2004) [16] method (Fig. 11b), some areas in the northeast (NE) of the study area are classified as "high" with respect to the liquefaction failure potential category. For the map constructed using the F_s obtained by the Moss et al. (2006) [18] method, an additional area located in the center of the study area is classified as "high" liquefaction failure potential. According to the maps shown in Fig 11, different failure potential categories and liquefaction susceptibility maps may be obtained from the different liquefaction evaluation methods due to the different F_s values.

6.2. Liquefaction Susceptibility Maps Based on Lee et al. (2003) Method

The liquefaction risk indices (I_R) calculated with Eq. 10 for all 28 CPT profiles in conjunction with four different CPT-based methods are given in Table 5. The liquefaction susceptibility maps prepared based on data listed in Table 5 are presented in Fig. 12.

Table 5. Liquefaction risk indices (I_R) calculated using four different CPT based methods.

CPT No	CPT coordinates		Liquefaction risk index, I_R			
	X	Y	Robertson & Wride (1998)	Boulanger & Idriss (2004)	Juang et al. (2006)	Moss et al. (2006)
1	549240	4288270	9.48	13.04	8.71	10.39
2	548480	4287920	2.68	4.86	2.62	3.55
3	549820	4288260	8.26	10.87	6.86	9.18
4	550070	4288260	11.80	16.01	9.15	14.25
5	550230	4287400	11.72	14.21	10.65	10.39
6	549710	4287430	6.36	9.66	7.30	9.50
7	549540	4286900	9.49	13.45	7.34	8.71
8	549120	4287570	10.80	13.33	10.01	13.57
9	548280	4287170	6.42	8.14	6.21	8.65
10	548740	4287590	6.30	7.93	5.29	8.34
11	548670	4286790	4.17	7.03	4.78	5.67
12	551000	4287430	9.51	12.09	6.56	9.37
13	551160	4287010	2.85	4.83	1.87	3.01
14	550770	4285710	9.48	11.65	8.44	11.34
15	551570	4286000	4.74	9.22	3.94	4.45
16	550490	4286600	0.73	2.35	0.65	1.61
17	551070	4285130	2.87	5.13	2.45	5.39
18	551290	4284680	6.12	9.94	7.36	8.81
19	551800	4285230	1.28	3.00	0.05	3.23
20	551770	4284320	1.38	2.03	0.46	1.42
21	549590	4286460	3.77	6.44	3.45	4.95
22	549150	4286500	4.22	8.17	4.32	5.05
23	547840	4286270	5.30	8.89	3.41	4.93
24	546800	4286190	4.25	6.02	4.23	5.19
25	546810	4286700	7.20	9.35	5.55	9.34
26	547170	4287470	1.65	3.98	0.98	4.28
27	547950	4287320	7.51	9.48	4.99	9.35
28	547570	4286840	2.90	4.40	2.77	4.70

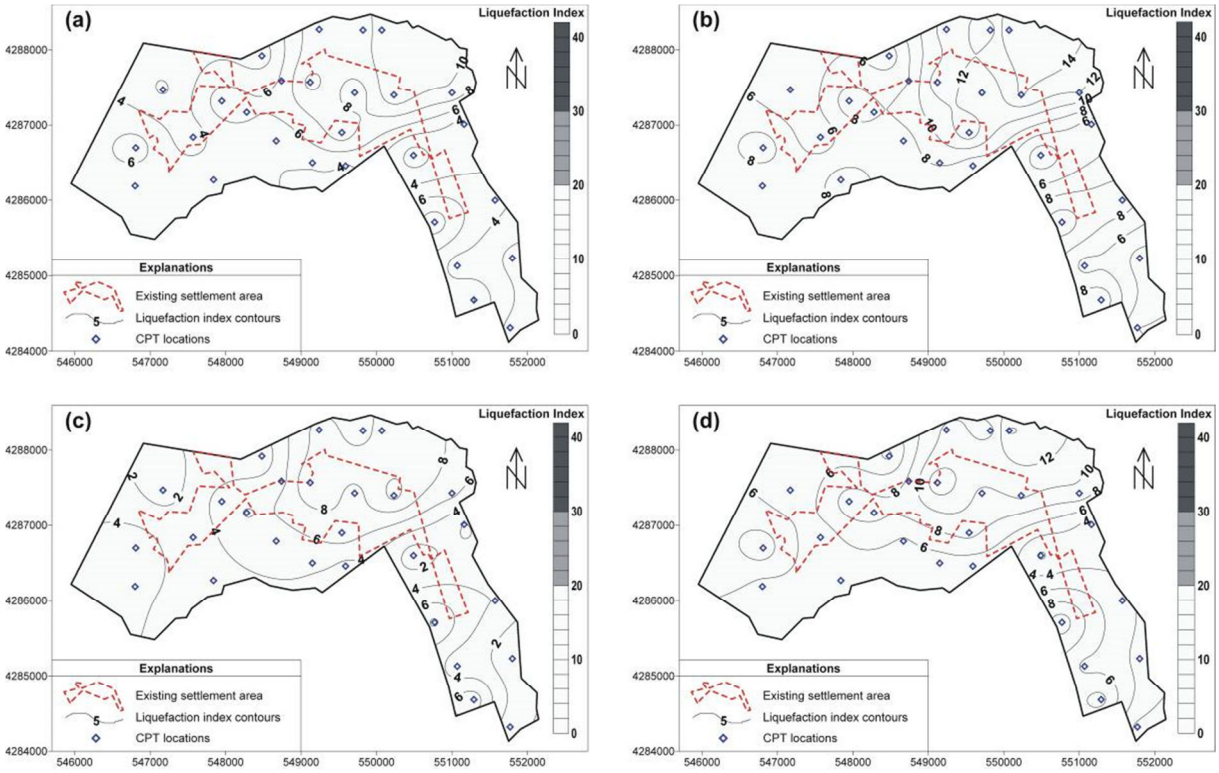

Figure 12. Liquefaction susceptibility maps based on Lee et al's (2003) [11] liquefaction risk index (IR) prepared in conjunction with the (a) Robertson and Wride (1998) [15]; (b) Boulanger and Idriss (2004) [16]; (c) Juang et al. (2006) [17]; and (d) Moss et al. (2006) [18] methods.

The liquefaction risk indices calculated by the equation proposed by Lee et al (2003) [11] (Eq. 10) using four CPT-based methods are less than 20 for all CPT profiles (Table 5). Therefore, as can also be seen from Figure 12, the entire study area is classified as "low" with respect to the liquefaction risk criteria suggested by Lee et al. (2003) [11] for all the CPT-based methods used in this study.

6.3. Liquefaction Susceptibility Maps Based on Sönmez and Gökceoğlu (2005) Method

The Liquefaction severity indices (I_S) calculated with Eq. 11 for all 28 CPT profiles in conjunction with four different CPT-based methods are listed in Table 6. Liquefaction susceptibility maps prepared based on the I_S values listed in Table 6 are presented in Fig. 13.

Table 6. Liquefaction severity index (I_S) calculated using four different CPT based methods.

CPT No	CPT coordinates		Liquefaction severity index, I_S			
	X	Y	Robertson & Wride (1998)	Boulanger & Idriss (2004)	Juang et al. (2006)	Moss et al. (2006)
1	549240	4288270	9.21	13.01	8.38	9.98
2	548480	4287920	2.36	4.74	2.41	3.09
3	549820	4288260	7.98	10.70	6.71	8.96
4	550070	4288260	11.35	15.85	8.89	13.92
5	550230	4287400	11.53	14.16	10.50	10.20
6	549710	4287430	6.25	9.62	7.20	9.37
7	549540	4286900	8.93	13.05	6.90	8.19
8	549120	4287570	10.70	13.29	9.97	13.54
9	548280	4287170	6.34	8.10	6.16	8.61
10	548740	4287590	6.23	7.89	5.24	8.30
11	548670	4286790	3.99	6.66	4.73	5.60
12	551000	4287430	9.24	11.69	6.31	9.09
13	551160	4287010	2.63	4.79	1.68	2.79
14	550770	4285710	9.40	11.61	8.39	11.30
15	551570	4286000	3.85	8.98	3.46	3.70
16	550490	4286600	0.44	2.18	0.40	1.34
17	551070	4285130	2.74	5.06	2.39	5.32
18	551290	4284680	5.68	9.87	7.30	8.75
19	551800	4285230	1.22	2.96	0.00	3.18
20	551770	4284320	1.27	1.97	0.39	1.34
21	549590	4286460	3.51	6.27	3.31	4.74
22	549150	4286500	3.75	7.84	4.01	4.61
23	547840	4286270	5.02	8.52	3.06	4.52
24	546800	4286190	3.99	5.75	4.12	5.04
25	546810	4286700	7.11	9.32	5.51	9.31
26	547170	4287470	1.55	3.94	0.94	4.24
27	547950	4287320	7.39	9.43	4.94	9.28
28	547570	4286840	2.84	4.36	2.73	4.66

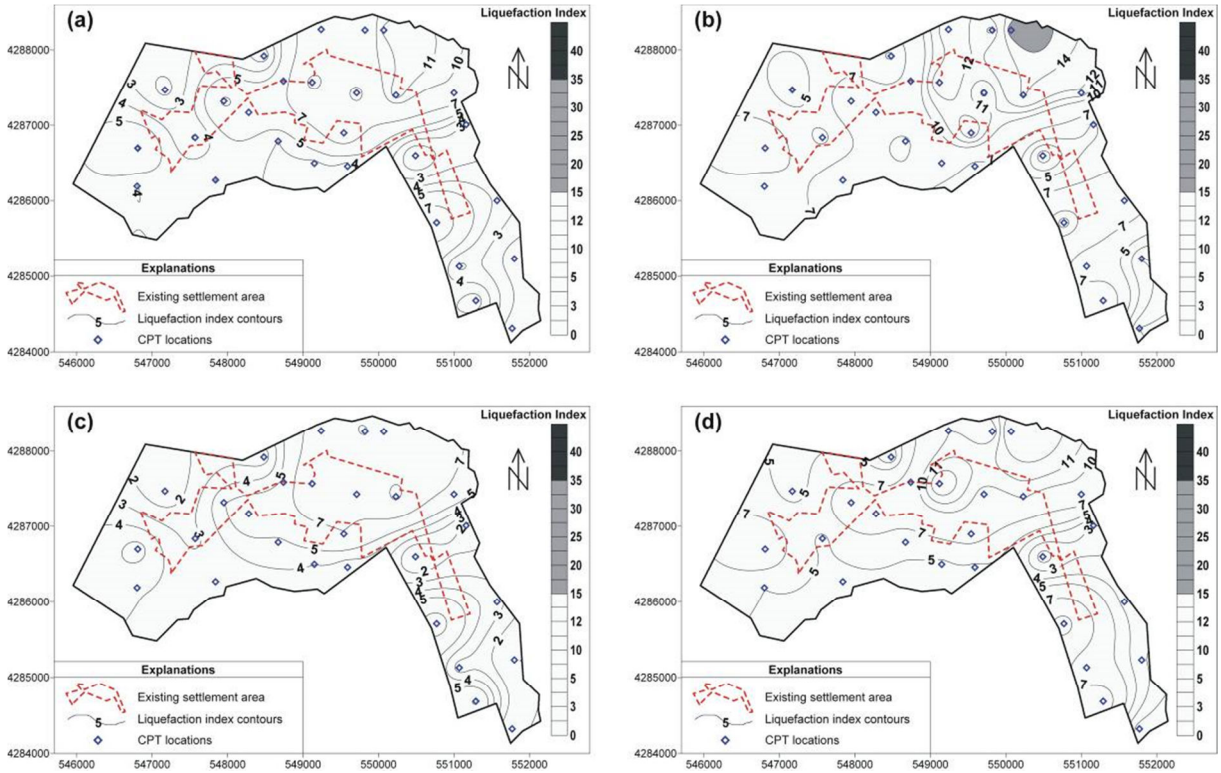

Figure 13. Liquefaction susceptibility maps based on Sönmez and Gökceoğlu's liquefaction severity index (I_S) constructed in conjunction with the (a) Robertson and Wride (1998) [15]; (b) Boulanger and Idriss (2004) [16]; (c) Juang et al. (2006) [17]; and (d) Moss et al. (2006) [18] methods.

As can be seen from Table 6, all indices are less than 15 except for CPT No.4, which was calculated using the Boulanger & Idriss (2004) [16] method. For the Robertson and Wride (1998) [15]; Juang et al. (2006) [17]; and Moss et al. (2006) [18] methods, the entire area is classified as "very low" according to the liquefaction failure potential criteria suggested by Sönmez and Gökceoğlu (2005) [29], while a small area located in the northeast (NE) of the study area is classified as "low" in conjunction with the Boulanger and Idriss (2004) [16] method.

By considering the maps shown in Figs 11, 12 and 13, it can be concluded that the liquefaction potential index (I_L) proposed by Iwasaki et al. (1982) [26] is more conservative than the other indices (i.e. I_R and IS) suggested by Lee et al. (2003) [11] and Sönmez and Gökceoğlu (2005) [29] based on CPT data gathered from the study site.

6.4. Liquefaction Susceptibility Maps That Reflects the Effect of Fluctuation of the GWT

It is well known that liquefaction only occurs in soils that are located below the groundwater table (GWT). Hence, it should be noted that at sites where the GWT fluctuates, the liquefaction potential will also fluctuate [30]. For this reason, in order to determine the effect of fluctuations of the GWT on the liquefaction potential of the study site, liquefaction susceptibility maps were constructed using varying depths of the GWT. The Robertson & Wride (1998) [15] method, in conjunction with the Iwasaki et al. (1982) [26] index, was used to calculate the liquefaction potential index for the construction of these maps. These maps are presented in Fig. 14.

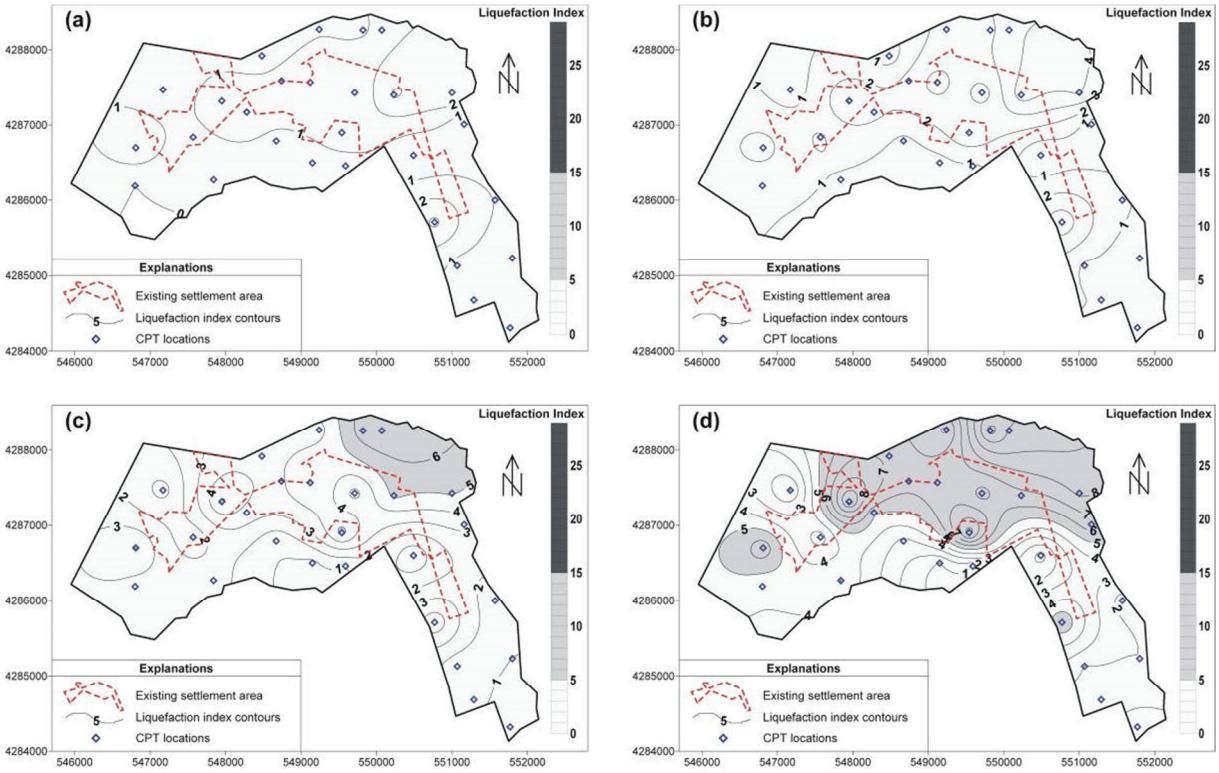

Figure 14. Liquefaction susceptibility maps prepared by using various ground water table depths at (a) 4 m; (b) 3 m; (c) 2; and (d) 1 m.

The liquefaction potential is classified as "low" for all study sites according to the Iwasaki et al (1982) [26] criteria for the GWT depths of 4 and 3 meters (Fig. 14a and b). When the level of the GWT rises to 2 m, a small region in the NE of the study site is classified as "high" (Fig. 14c). However, when the GWT rises to 1 meter depth, the liquefaction failure potential of a considerably larger part of the study site was assessed as "high" (Fig. 14d).

According to the results shown in Fig. 14, fluctuations of the GWT should be considered during the planning stage of the new settlement areas.

6.5. Ground Settlement Maps of the Study Site

Liquefaction-induced ground settlements are essentially vertical deformations of surficial soil layers caused by the densification and compaction of loose granular soils following earthquake loading [20]. Field test-based methods are widely used for the estimation of liquefaction-induced ground settlement for low to medium risk projects and also to provide preliminary estimates for higher risk projects. In this study, ground settlements due to liquefaction were estimated using CPT-based methods in conjunction with the results of Ishiara and Yoshimine (1992) [31].

Ishiara and Yoshimine (1992) [31] proposed a family of curves based mainly on results from laboratory tests conducted on Fuji River sand for obtaining post-liquefaction volumetric strain (Fig. 15a). Zhang et al. (2002) [20] correlated the curves proposed by Ishiara and Yoshimine (1992) [31] with relative density (D_r) and the F_s against liquefaction for clean sands (Fig. 15b). They then developed correlations between $(q_{c1N})_{cs}$ and postliquefaction volumetric strain for different F_s on the basis of the curves of Ishiara and Yoshimine (1992) [31]. The resulting curves obtained by Zhang et al. (2002) [20] from these correlations are given in Fig.15(b).

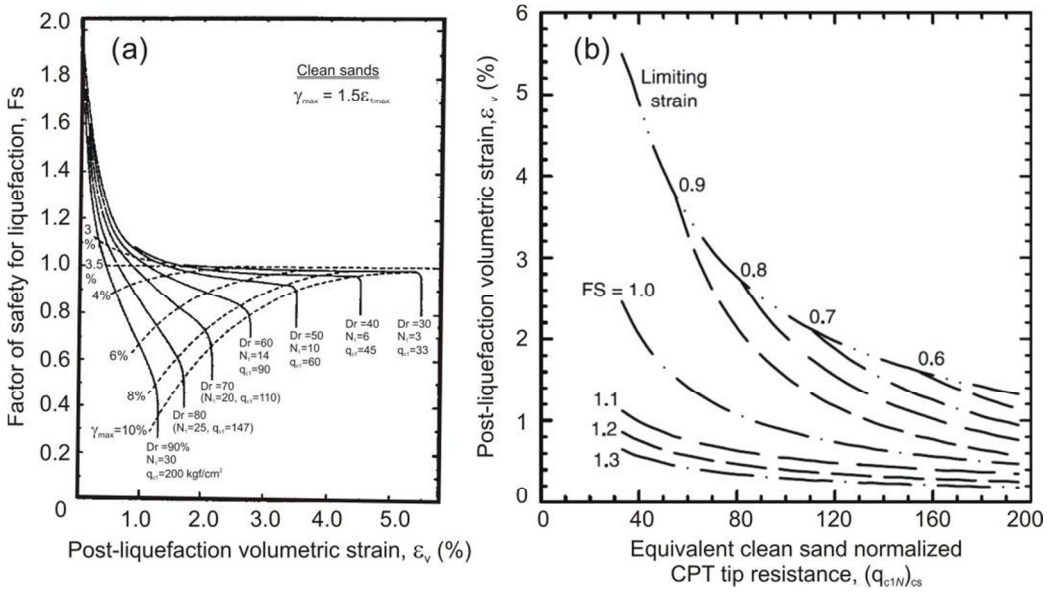

Figure 15. (a) Charts for determining volumetric strain as functions of factor of safety (Ishiara and Yoshimine, 1992 [31]), (b) Relationship between postliquefaction volumetric strain and equivalent clean sand normalized CPT tip resistance for different factors of safety [20].

The equivalent clean sand normalized CPT penetration resistance, $(q_{c1N})_{cs}$ and F_s for sandy and silty soils can be obtained from the CPT-based liquefaction potential analysis proposed by Robertson and Wride (1998) [15]. The post-liquefaction volumetric strain can then be estimated using Fig. 15(b) for every reading in the CPT sounding. Thereafter, liquefaction-induced ground settlement at the CPT location due to the design earthquake can then be estimated by the following equation;

$$S = \sum_{i=1}^{j} \varepsilon_{vi} \, \Delta z_i \qquad (12)$$

where S is the calculated liquefaction-induced ground settlement at the CPT location; ε_{vi} is the post-liquefaction volumetric strain for the soil sub-layer i; Δz_i is the thickness of the sub-layer i; and j is the number of soil sub-layers.

In this study, expected ground settlements due to soil liquefaction after the design earthquake were estimated with Eq. 12 in conjunction with four different CPT-based methods. The results obtained from these analyses are listed in Table 7 and settlement maps of the study site constructed with these data are given in Fig. 16.

Skempton and MacDonald (1956) [32] proposed 5.1 cm as a maximum differential settlement for isolated foundations on sands. Therefore liquefaction settlement greater than 5 cm was evaluated as a critical value for structural damage. Hence, in Fig. 16, settlement values between 5 and 10 cm is indicated with a gray color whereas settlement values greater than 10 cm is indicated with a black color for easy evaluation.

Table 7. Ground settlements calculated in conjunction with four different CPT-based methods.

CPT No	CPT coordinates		Ground settlements (cm)			
	X	Y	Robertson & Wride (1998)	Boulanger & Idriss (2004)	Juang et al. (2006)	Moss et al. (2006)
1	549240	4288270	3.70	7.60	4.46	5.74
2	548480	4287920	0.84	2.41	1.24	1.66
3	549820	4288260	3.54	6.39	3.95	5.55
4	550070	4288260	5.12	10.89	5.87	9.62
5	550230	4287400	5.63	7.34	5.89	6.02
6	549710	4287430	2.33	6.35	4.26	5.93
7	549540	4286900	4.20	6.74	3.89	5.04
8	549120	4287570	4.76	9.06	5.96	8.65
9	548280	4287170	2.87	5.84	3.95	5.83
10	548740	4287590	3.01	6.02	3.50	6.02
11	548670	4286790	1.43	3.81	2.54	3.10
12	551000	4287430	5.21	7.64	3.96	6.56
13	551160	4287010	0.93	2.40	0.78	1.50
14	550770	4285710	5.80	9.93	6.78	9.91
15	551570	4286000	1.60	3.36	1.86	2.21
16	550490	4286600	0.17	1.11	0.23	0.84
17	551070	4285130	1.34	4.32	1.82	4.25
18	551290	4284680	1.85	5.01	3.26	4.17
19	551800	4285230	0.37	2.26	0.00	2.26
20	551770	4284320	0.57	1.42	0.23	1.14
21	549590	4286460	1.28	3.53	1.76	2.85
22	549150	4286500	1.30	4.09	2.17	2.67
23	547840	4286270	1.77	4.46	1.31	2.46
24	546800	4286190	1.67	3.08	2.21	2.78
25	546810	4286700	3.08	6.18	3.05	5.90
26	547170	4287470	0.64	2.82	0.56	2.82
27	547950	4287320	4.03	7.75	3.65	7.56
28	547570	4286840	1.19	3.22	1.72	3.22

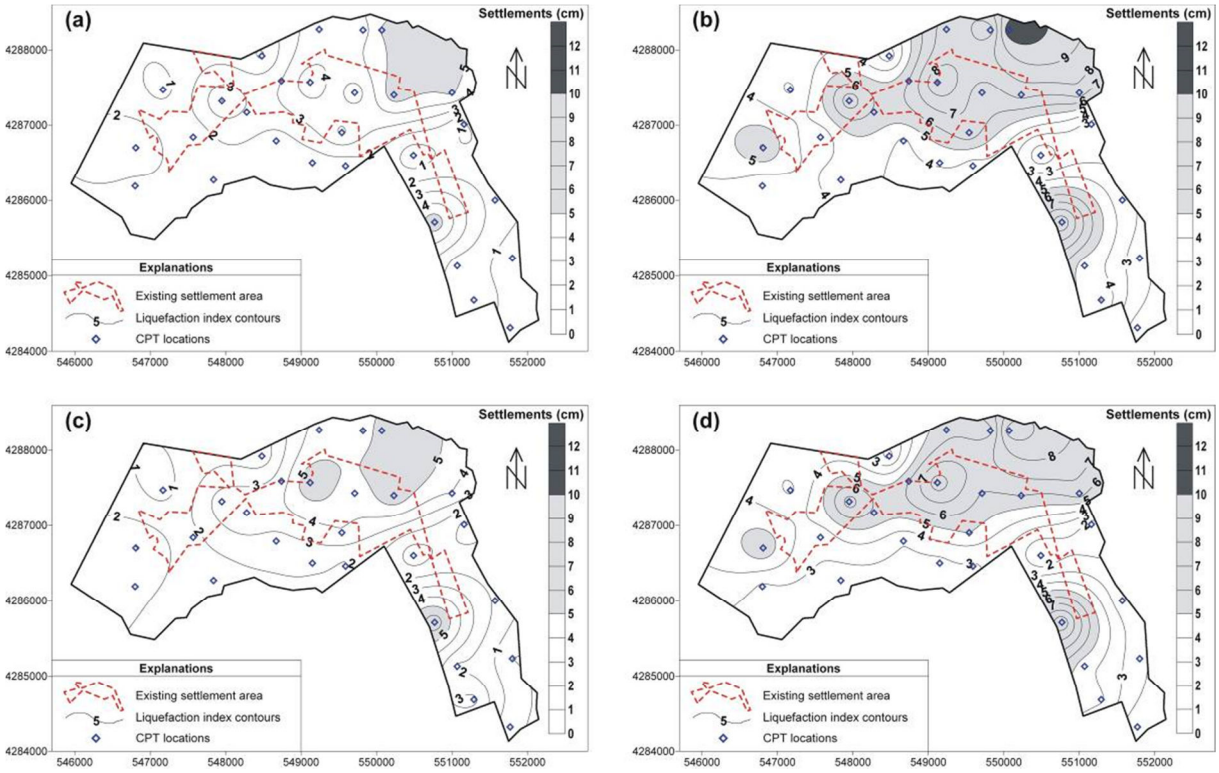

Figure 16. Ground settlement maps of the study area; Liquefaction potential and factor of safety against liquefaction were calculated by the (a) Robertson and Wride (1998) [15]; (b) Boulanger and Idriss (2004) [16]; (c) Juang et al. (2006) [17]; and (d) Moss et al. (2006) [18] methods.

The settlement maps prepared by different CPT-based methods are considerably different. When the factor of safety against liquefaction was calculated with Robertson and Wride's (1998) [15] method, settlements between 5 and 10 cm were estimated for a small area located NE of the study site (Fig. 16a). However, when the Boulanger and Idriss (2004) [16] method was used to calculate the factor of safety against liquefaction, settlements greater than 10 cm were estimated for a small area located NE of the study site, in addition to areas in which settlements between 5 and 10 cm were expected (Fig. 16b). When the Juang et al. (2006) [17] method was used to calculate the factor of safety against liquefaction, settlements between 5 and 10 cm were estimated for an additional small area located in the center and SW of the study site (Fig. 16c). When using the Moss et al. (2006) method [18], settlements between 5 and 10 cm were estimated for a large area (Fig. 16d).

According to the maps shown in Fig. 16, more conservative results were obtained from the Boulanger and Idriss (2004) [16] method (Fig. 16b). When the Boulanger and Idriss (2004) [16] method was used, the area in which settlements greater than 5 cm, are larger than area estimated from the other methods. Besides, almost similar settlement maps were obtained from Moss et al. (2006) [18] and Boulanger and Idriss (2004) [16] methods.

In a recent study, Çetin et al. (2009) [33] proposed a methodology for the calculation of cyclic reconsolidation settlement of saturated cohesionless soil sites. In that study, volumetric strain is calculated using the corrected cyclic stress ratio ($CSR_{SS,20,1D,1\ atm}$) and corrected SPT blow counts ($N_{1,60,CS}$). This methodology did not cover the CPT tip resistance. Therefore, the methodology proposed by Çetin et al. (2009) [33] cannot be used in this study because tip resistance values should be converted to $N_{1,60,CS}$, and this conversion will cause additional uncertainties. Çetin et al. (2009) [33] also assessed the performance of existing procedures for the estimation of cyclic reconsolidation settlements of saturated cohesionless soil sites. They indicated that the methodology proposed by Ishiara and Yoshimine (1992) [31] overestimates the actual settlements by about 10 %.

CONCLUSIONS

In this study, liquefaction susceptibility maps were prepared for regions covered by alluvial deposits in the Saruhanlı-Manisa area of Turkey using different liquefaction index approaches and four different widely used CPT-based methods. As a result, the most conservative case was obtained in the case of using the liquefaction potential index (I_L) proposed by Iwasaki et al. (1982) [26] for the evaluation of liquefaction potential risk of the site. The maps obtained from the different indices and methods, showed that different risk levels can be obtained for a site by using different

liquefaction indices and different CPT-based methods. Thus, when evaluating the liquefaction potential of a site, several widely used liquefaction assessment methods should be considered for the study site. Remedial measures against soil liquefaction and associated ground failures should then be taken by considering the liquefaction susceptibility map that reflects the worst case.

In addition, by considering fluctuations of the GWT in the study site, liquefaction susceptibility maps were constructed using varying depths of the GWT from 4 meters to the ground surface. It was determined that when the GWT rises, the liquefaction failure potential of the study site increased considerably. Based on this result, it was concluded that the fluctuations of the GWT should be considered during the planning stage of the new settlement areas.

Finally, settlement maps of the study site were constructed with the data obtained from different CPT-based liquefaction assessment methods. Hence, it was seen that different settlement maps can be obtained for a site by using different CPT-based liquefaction assessment methods. As a result, the most conservative case associated with the ground settlement due to liquefaction was obtained in the case of using the Boulanger and Idriss (2004) [16] method for the evaluation of liquefaction potential of the study site.

ACKNOWLEDGEMENTS

This study was funded by Gazi University Department of Scientific Research Projects (BAP) with a project no 07/2005-32. The authors would like to thank the staff of this department. The authors would also like to thank the staff of Iller Bankası for sharing the geotechnical data obtained from the site of Saruhanlı-Manisa area of Turkey in conjunction with Report No. ILB-I/45-039-004.

REFERENCES

[1] KOERI-NEMC, Bogaziçi University Kandilli Observatory and Earthquake Research Institute (KOERI), National Earthquake Monitoring Center (NEMC), available at http://www.koeri.boun.edu.tr/sismo/default.htm (accessed on 5 April 2010).

[2] Çiftçi, N.B., and Bozkurt, E., "Pattern of normal faulting in the Gediz Graben, SW Turkey", ***Tectonophysics***, 473(1-2): 234-260, (2009).

[3] Çiftçi, N.B., and Bozkurt, E., "Evolution of the miocene sedimentary fill of the Gediz Graben, SW Turkey", ***Sedimentary Geology***, 216(3-4): 49 – 79, (2009).

[4] Metli, F., Tan, T., Baykul, A., Akalin, H.L., Avsar, M., Turkbilegi, H., Sun, A., Saygili, N., Isin, R., "Environment geology and area usage potential of Manisa city and its vicinity", ***Geological Investigations Department, MTA***, Ankara, Report No. 10480 (in Turkish), (2001).

[5] Sari, C., "Inversion of gravity data using singular value decomposition technique and determination of the sediment thicknesses of the Gediz and Buyuk Menderes Grabens", ***DEÜ Journal of Scienc and Engineering***, 5(13): 121 – 135 (in Tukish), (2003).

[6] Şengör, A.M.C., Yılmaz, Y., Sungurlu, O., "Tectonics of the Mediterranean Cimmerides: Nature and evolution of the western termination of Paleo-Tethys", In: Dixon J.E., Robertsen A.H.F., (Eds.), The Geological Evolution of the Eastern Mediterranean, ***Spec. Publ., Geol. Soc***. London, 17: 77–112 (1984).

[7] Sayisal Grafik, available at http://www.sayisalgrafik.com.tr/deprem/tr_frames.htm, (Accessed on 12 May 2009).

[8] Wells, D.L., Coppersmith, K.J., "New empirical relationships among magnitude, rupture length, rupture width, rupture area, and surface displacement", ***Bulletin of the Seismological Society of America***, 84(4): 974–1002, (1994).

[9] Ulusay, R., and Tuncay, E., Sonmez, H., and Gokceoglu, C., "An attenuation relationship based on Turkish strong motion data and iso-acceleration map of Turkey", ***Engineering Geology,*** 74: 265–291, (2004).

[10] Seed, H.B., Idriss, I.M., "Simplified procedure for evaluating soil liquefaction potential", ***Journal of Geotechnical Engineering***, ASCE, 97(9): 1249-1273, (1971).

[11] Lee, D.H., Ku, C.S., Yuan, H., "A study of the liquefaction risk potential at Yuanlin, Taiwan", ***Engineering Geology***, 71: 97–117, (2003).

[12] Bulut, İ., Sağlam, M., Bektaş, İ.A., Şahin, M.S., Demir, M., Uran, Ş., Üçkardeşler, C., Güner, F., Araz, A.H., "Geological and geotechnical report of the sites requiring detailed geotechnical investigations for the town planning of Saruhanlı (Manisa) municipality", Report No. ILB-I/45-039-004 , Ankara-Turkey (in Turkish), (2006).

[13] Tsuchida, H., "Prediction and countermeasure against liquefaction in sand deposits", ***Abstract of the Seminar of the Port and Harbour Research Institute***, Ministry of Transport, Yokosuka, Japan, 3.1–3.33 (in Japanese), (1970).

[14] Youd, T.L, et al., "Liquefaction resistance of soils: Summary report from the 1996 NCEER and 1998 NCEER/NSF workshops on evaluation of liquefaction resistance of soils", ***Journal of Geotechnical and Geoenvironmental Engineering***, ASCE; 127(10):817–833, (2001).

[15] Robertson, P.K., Wride (Fear), C.E., "Evaluating cyclic liquefaction potential using the cone penetration test", ***Canadian Geotechnical Journal***, 35(3): 442–459, (1998).

[16] Boulanger, R.W., Idriss, I.M., "State normalization of penetration resistance and the effect of overburden stress on liquefaction

resistance", Proceedings 11th International Conference on Soil Dynamics and Earthquake Engineering and 3rd International Conference on Earthquake Geotechnical Engineering. Univ. of California, Berkeley, CA, 2: 484–491, (2004).

[17] Juang, C.H., Fang. S.Y., Khor. E.H., "First-Order Reliability Method for Probabilistic Liquefaction Triggering Analysis Using CPT", ***Journal of Geotechnical and Geoenvironmental Engineering,*** 132 (3): 337–350, (2006).

[18] Moss, R.E.S., Seed, R.B., Kayen, R.E., Stewart, J.P., Der Kiureghian, A., Cetin, K.O., "CPT-Based probabilistic and deterministic assessment of in situ seismic soil liquefaction potential", ***Journal of Geotechnical and Geoenvironmental Engineering***, 132(8): 1032–1051, (2006).

[19] Robertson, P.K., "Estimation of minimum undrained shear strength for flow liquefaction using the CPT", In: P. Sêco e Pinto (Ed.), Earthquake geotechnical engineering, Balkema, Rotterdam, 1021–1028, (1999).

[20] Zhang, G., Robertson, P.K., Brachman, R.W.I., "Estimating liquefaction-induced ground settlements from CPT for level ground", ***Canadian Geotechnical Journal***, 39(5): 1168–1180, (2002).

[21] Liao, S.S.C., Whitman, R.V., "Catalogue of A Liquefaction and Non-Liquefaction Occurrences During Earthquakes", ***Research Report, Department of Civil Engineering***, Massachusetts Institute of Technology, Cambridge, Mass, (1986).

[22] Seed, H.B., Idriss, I.M., "Ground motions and soil liquefaction during earthquakes", ***Earthquake Engineering Research Institute Monograph***, Oakland, California, (1982).

[23] Hynes, M.E., Olsen, R.S., "Influence of confining stress on liquefaction resistance", ***Proceeding International Workshop on Physics and Mechanics of Soil Liquefaction***, Balkema, Rotterdam, The Netherlands, 145-152, (1999).

[24] Idriss, I.M., Boulanger, R.W., "Semi-empirical procedures for evaluating liquefaction potential during earthquakes", ***Soil Dynamics and Earthquake Engineering***, 26(2-4): 115–130, (2006).

[25] Çetin, K.O., Seed, R.B., Der Kiureghian, A., Tokimatsu, K., Harder, L.F., Jr. Kayen, R.E., Moss, R.E.S., "Standard penetration test-based probabilistic and deterministic assessment of seismic soil liquefaction potential", ***Journal of Geotechnical and Geoenvironmental Engineering***. 130(12): 1314–1340, (2004).

[26] Iwasaki, T., Tokida, K., Tatsuoka, F., Watanabe, S., Yasuda, S., Sato, H., "Microzonation for soil liquefaction potential using simplified methods", ***In: Proceedings of the 3th International Conference on microzonation***, Seattle, USA, 3: 1319–1330, (1982).

[27] JSHE, Highway Bridge Design Guide Book, ***Japan Society of Highway Engineering***, Tokyo (In Japanese), (1990).

[28] Juang, C.H., Yuan, H., Lee, D.H., Lin, P.S., "A simplified cone penetration test–based method for evaluating liquefaction potential of soils", ***Journal of Geotechnical and Geoenvironmental Engineering***, 129(1): 66–80, (2003).

[29] Sönmez, H., Gökçeoğlu, C., "A liquefaction severity index suggested for engineering practice", ***Environmental Geology,*** 48: 81–91, (2005).

[30] Day, R.W., "Geotechnical Earthquake Engineering Handbook", ***McGraw-Hill Company Inc.***, U.S.A, (2002).

[31] Ishihara, K., Yoshimine, M., "Evaluation of settlements in sand deposits following liquefaction during earthquakes", ***Soils and Foundations,*** 32(1): 173–188, (1992).

[32] Skemton, A.W and MacDonald, D.H., "The allowable settlement of buildings", *ICE Proceedings: Engineering Divisions*, 5(6): 727–768, (1956).

[33] Çetin, K.O., Bilge, H.T., Wu, J., Kammerer, A.M., Seed R.B., "Probabilistic model for the assessment of cyclically induced reconsolidation (volumetric) settlements", *Journal of Geotechnical and Geoenvironmental Engineering*. 135(3): 387–398, (2009).